Strong coupling between antiferromagnetic and superconducting order parameters of $CeRhIn_5$ studied by ^{115}In nuclear quadrupole resonance spectroscopy

M. Yashima,[1] H. Mukuda,[1] Y. Kitaoka,[1] H. Shishido,[2,*] R. Settai,[2] and Y. Ōnuki[2,3]
[1]*Department of Materials Engineering Science, Osaka University, Osaka 560-8531, Japan*
[2]*Department of Physics, Graduate School of Science, Osaka University, Osaka 560-0043, Japan*
[3]*Advanced Science Research Center, Japan Atomic Energy Research Institute, Tokai, Ibaraki 319-1195, Japan*
(Received 9 December 2008; revised manuscript received 18 March 2009; published 25 June 2009)

We report on a pressure (P)-induced evolution of magnetism and superconductivity (SC) in a helical magnet $CeRhIn_5$ with an incommensurate wave vector $Q_i=(\frac{1}{2},\frac{1}{2},0.297)$ through the ^{115}In nuclear quadrupole resonance (NQR) measurements under P. Systematic measurements of the ^{115}In-NQR spectrum reveal that the commensurate antiferromagnetism (AFM) with $Q_c=(\frac{1}{2},\frac{1}{2},\frac{1}{2})$ is realized above $P_m\sim 1.7$ GPa. An important finding is that the size of SC gap and T_c increase as the magnitude of the AFM moment decreases in the P region, where SC uniformly coexists with the commensurate AFM. This result provides evidence of strong coupling between the commensurate AFM order parameter (OP) and SC OP.

DOI: 10.1103/PhysRevB.79.214528 PACS number(s): 74.25.Ha, 74.62.Fj, 74.70.Tx, 75.30.Kz

I. INTRODUCTION

Various studies on the Ce115 family have revealed an intimate relationship between antiferromagnetism (AFM) and superconductivity (SC). $CeRhIn_5$ is a heavy-fermion helical magnet with $Q_i=(\frac{1}{2},\frac{1}{2},0.297)$ and Néel temperature $(T_N)=3.8$ K at an ambient pressure ($P=0$), as shown in Fig. 1(a),[1] and it exhibits P-induced SC.[2–5] Previous ^{115}In-nuclear quadrupole resonance (NQR) experiments on $CeRhIn_5$ have unraveled a homogeneously coexisting state of AFM and SC in the range of $P=1.6$–2.1 GPa. In this novel state of matter, a quantum critical point (QCP)—the point at which AFM collapses—and a tetracritical point in the pressure-temperature phase diagram have been found to be around $P_{QCP}=2.1$ GPa and $P_{tetra}=1.98$ GPa, respectively.[6–8] A neutron-diffraction experiment performed at P indicates that the helical structure is maintained at 1.63 GPa,[9] while other reports state that $Q_{iz}=0.297$ at $P=0$ suddenly changes into $Q_{iz}\sim 0.4$ near $P=1$ GPa.[10,11] The $CeRh_{1-x}Ir_xIn_5$ system exhibited a commensurate AFM with $Q_c=(\frac{1}{2},\frac{1}{2},\frac{1}{2})$ in the P range where SC occurs, in addition to exhibiting a helical order similar to that in $CeRhIn_5$. This result suggested an intimate relationship between the onset of SC and the development of a magnetic structure during the coexistence of AFM and SC.[12] Commensurate AFM was also reported in $CeRh_{1-x}Co_xIn_5$.[13,14] The magnetically ordered Ce moment $M_Q=0.8\mu_B$ at $P=0$ was reported to slightly decrease to $\sim 0.67\mu_B$ at $P=1.63$ GPa (Ref. 9); a recent experiment[11] reported $M_Q=0.6$ and $0.43\mu_B$ at $P=0$ and in the range of 1.5–1.7 GPa, respectively. However, no magnetic structure has so far been observed in the uniformly coexisting phase of AFM and SC in $P=1.6$–2.1 GPa.

In this paper, we report on the P-induced evolution of the magnetic structure and its relation to SC through systematic ^{115}In-NQR studies at the In(1) and the In(2) sites in $CeRhIn_5$. It is revealed that commensurate AFM with $Q_c=(\frac{1}{2},\frac{1}{2},\frac{1}{2})$ is induced above $P\sim 1.7$ GPa. The present experiments show the strong coupling between AFM and SC order parameters (OPs).

II. EXPERIMENTAL PROCEDURE

The single crystals of $CeRhIn_5$ grown by the self-flux method were moderately crushed into coarse powder in order to allow the rf pulses to easily penetrate the sample for NQR measurements. Hydrostatic pressure was applied by utilizing a NiCrAl-BeCu piston-cylinder cell that was filled with Si-based organic liquid as the pressure-transmitting medium.[16] To calibrate the pressure at low temperatures, the shift in T_c of Sn metal at P was monitored by the resistivity measurements. The measurements of the $^{115}In(I=9/2)$-NQR spectrum were performed at the transition of $3\nu_Q$ for the $^{115}In(2)$ site in $CeRhIn_5$. $CeRhIn_5$ consists of alternating layers of CeIn and $RhIn_4$, as indicated in Fig. 1(a), and there are two sites—In(1) and In(2)—per unit cell. The In(1) and the In(2)

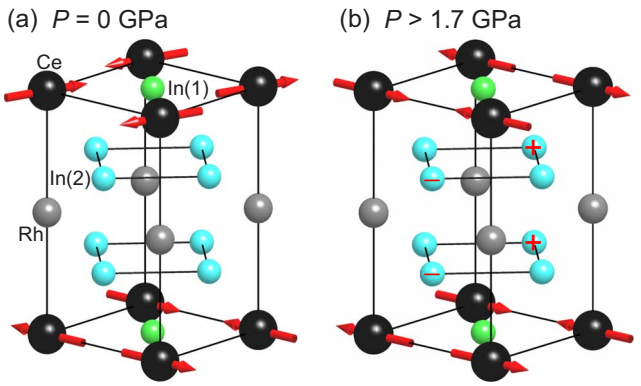

FIG. 1. (Color online) Crystal and magnetic structures of $CeRhIn_5$. (a) The incommensurate helical structure along the c axis with $Q_i=(1/2,1/2,0.297)$ at $P=0$. (b) The commensurate antiferromagnetic structure starts to appear under P. In this magnetic structure, there are two magnetically different In(2) sites, as shown in this figure. One of these sites considers H_{int} with a "+" or a "−" sign against the direction of M_Q and the other site considers $H_{int}=0$. As discussed in Ref. 15 the H_{int} at the In(2) site also originates from the direct dipolar field from the Ce magnetic moments and from the indirect "pseudodipolar" anisotropic field via the super-transferred hyperfine interaction due to the hybridization between the In-5p and Ce-4f orbits.

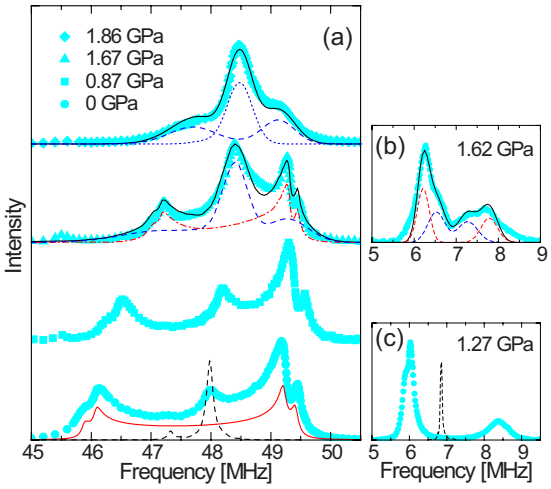

FIG. 2. (Color online) (a) The P dependence of the NQR spectrum on the magnetically ordered state in $CeRhIn_5$ at the In(2) site (the $3\nu_Q$ transition). It was measured at $T=1.5$ K, well below T_N. The dashed line at $P=0$ indicates the NQR spectra of the paramagnetic spectrum measured at $T=4.2$ K. At $P=1.67$ GPa, the dashed and the dotted-dashed lines indicate the simulated spectra for the commensurate AFM and the incommensurate helical order, respectively. The solid line represents the convolution of them with fractions of 0.6 and 0.4, respectively. At $P=1.86$ GPa, the solid line represents a simulated spectrum for the commensurate AFM; the two peaks indicated by the dashed line represent the In(2) sites with $H_{\rm int}=\pm 1.1$ kG, which are indicated by "+" and "−" signs in Fig. 1(b). The dotted line is the simulated spectrum for the In(2) site with $H_{\rm int}=0$. (b) The spectrum of the $1\nu_Q$ transition at the In(1) site, $T=0.2$ K, and $P=1.62$ GPa. The spectrum is well simulated similar to that at In(2) at $P=1.67$ GPa in (a). (c) The spectrum of the $1\nu_Q$ transition at the In(1) site, $T=0.6$ K, and $P=1.27$ GPa. The spectrum in the paramagnetic state at 4.2 K is indicated by the dashed line.

sites are located in the CeIn and the $RhIn_4$ layers, respectively. Here, ν_Q is defined by the NQR Hamiltonian, $\mathcal{H}_Q=(h\nu_Q/6)[3I_z^2-I(I+1)+\eta(I_x^2-I_y^2)]$, where η is the asymmetry parameter of the electric-field gradient [$\nu_Q=16.656$ MHz and $\eta=0.445$ at the In(2) site; $P=0$ and $T=4.2$ K]. When an internal magnetic field $H_{\rm int}(\propto M_Q)$ is present at the In sites in association with the onset of AFM, the NQR Hamiltonian is perturbed by the Zeeman interaction, which is given by $\mathcal{H}_{\rm AFM}=-\gamma\hbar\vec{I}\cdot\vec{H}_{\rm int}+\mathcal{H}_Q$. The onset of AFM is signaled by the splitting of the NQR spectrum by $H_{\rm int}$.

III. RESULTS AND DISCUSSION

Figure 2(a) shows the P dependence of the NQR spectrum (the $3\nu_Q$ transition) on the In(2) site in the magnetically ordered state of $CeRhIn_5$. Since M_Q rotates about the c axis with $Q_i=(\frac{1}{2},\frac{1}{2},0.297)$, the amplitude of $H_{\rm int}$ at the In(2) site varies along the axis. As a result, the NQR spectrum at $P=0$ exhibits a very broad pattern [see the spectrum at the bottom of Fig. 2(a)]. This spectrum at $P=0$ is well simulated, assuming $H_{\rm int}=H_{\rm max}\cos(2\pi Q_{iz}z)$ as given in Ref. 17. The solid line in the spectrum for $P=0$ in Fig. 2(a) represents the distribution $R(\omega)$ of the NQR frequency for $H_{\rm max}=2.5$ kG including an inhomogeneous broadening $\sigma=120$ kHz (Lorentzian function). Here, $R(\omega)=\Sigma_{\omega_k}f(\omega_k)\frac{\sigma^2}{4(\omega-\omega_k)^2+\sigma^2}$ and $f(\omega)$ is the distribution of the NQR frequency obtained from the distribution of $H_{\rm int}$ through $\mathcal{H}_{\rm AFM}=-\gamma\hbar\vec{I}\cdot\vec{H}_{\rm int}+\mathcal{H}_Q$. However, the NQR spectrum at $P=0$ exhibits a central peak that does not exist in the simulation (solid line), indicating the existence of either a paramagnetic (PM) phase or different magnetic phases even at $P=0$. In order to examine the possible contamination of a paramagnetic phase, we present the NQR spectrum (the $1\nu_Q$ transition) in Fig. 2(c) at the In(1) site at $T=0.6$ K, which is lower than $T_N=3.8$ K. If such a phase exists in the sample, the spectrum shown by the dashed line should be observed. The well-articulated NQR spectrum with two peaks at the In(1) site excludes paramagnetic phases. As demonstrated later, the central peak in the In(2)-NQR spectrum at $P=0$ shown in Fig. 2(a) arises from commensurate AFM domains shown in Fig. 1(b). Incidentally, it is confirmed from the In(2)-NQR spectrum measurements that the volume fraction of the incommensurate AFM changes negligibly below T_N (the complete data are not shown here).

We focus on a systematic P-induced evolution of the NQR spectrum. The NQR spectral shape does not change much at pressures up to 0.87 GPa, except for a slight increase in the intensity of the central peak. As P exceeds 1.6 GPa, however, the NQR intensity at the central peak also increases significantly. Eventually, the spectral shape that is inherent to the helical order disappears at $P=1.86$ GPa [see the spectrum at the top of Fig. 2(a)]. Since paramagnetic phases are excluded from the NQR spectrum at the In(1) site as mentioned above, such a drastic change in the NQR spectrum indicates a P-induced change in the AFM structure of $CeRhIn_5$. In fact, the NQR spectral shape at $P=1.86$ GPa is well interpreted by assuming the commensurate AFM with $Q_c=(\frac{1}{2},\frac{1}{2},\frac{1}{2})$ shown in Fig. 1(b). In this AFM structure, there are two magnetically different In(2) sites, as shown in Fig. 1(b). One of them considers $H_{\rm int}$ with a "+" or a "−" sign that indicates the up or the down direction, respectively, of $\vec{H}_{\rm int}$ along the c axis at each In(2) site, and the other site considers $H_{\rm int}=0$. The characteristic spectrum at $P=1.86$ GPa is thus well simulated with $H_{\rm int}=1.1$ kG, as represented by the solid line in the spectrum at the top of Fig. 2(a), thereby demonstrating that the commensurate AFM shown in Fig. 1(b) occurs near the AFM-QCP in $CeRhIn_5$. It is to be noted that the volume fraction of the commensurate AFM domains (VF_c) increases slightly up to 1 GPa and reaches 100% at 1.76 GPa, as shown in Fig. 3(b). This reveals that the incommensurate AFM completely changes into the commensurate AFM around $P_m\sim 1.7$ GPa. The four peaks in the In(1) spectrum at 1.62 GPa shown in Fig. 2(b) were reported in a previous paper.[8] The present NQR measurements suggest that the four peaks are associated with the combination of the commensurate and the incommensurate AFMs just below P_m. The difference in $H_{\rm int}$ between the commensurate and incommensurate AFMs may be due to the difference in the hyperfine coupling. VF_c is estimated at 1.62 GPa from the analysis of the spectrum at the In(1) site, as shown in Fig. 2(b), and it is denoted by an open triangle in Fig. 3(b).

We study the P-induced evolution of $H_{\rm int}$ at the In(2) site. Figure 3(c) indicates that $H_{\rm int}$ progressively decreases from

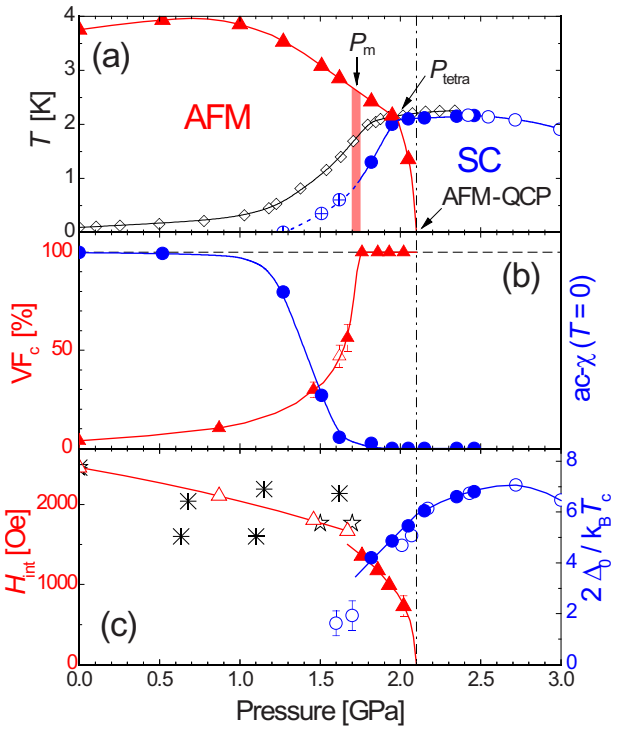

FIG. 3. (Color online) (a) The phase diagram of $CeRhIn_5$. T_N (triangles) and T_c (solid circles and encircled crosses) are determined from the In-NQR-$1/T_1$ measurement. The encircled cross indicates T_c for the incommensurate AFM. The P dependence of T_c (diamonds) is determined from the susceptibility measurement performed using a single crystal (Ref. 18). The open circle indicates T_c obtained from the specific-heat measurements (Ref. 4). The solid lines are guides to the eyes. P_{tetra} indicates the pressure at the tetracritical point separating AFM, AFM+S, SC, and PM phases. AFM-QCP points to the quantum critical point at which the AFM collapses. The commensurate AFM is completely realized at P_m. (b) The P dependences of VF_c (triangles) and the SC diamagnetism extrapolated to $T=0$ (circles). The open triangle at 1.62 GPa is estimated from the analysis of the spectrum at the In(1) site, as shown in Fig. 2(b). The solid lines are guides to the eyes. (c) The P dependences of H_{int} on the In(2) sites for the incommensurate AFM (△) and the commensurate AFM (▲) along with those of M_Q (∗ and ☆) obtained from neutron-scattering experiments (Refs 9 and 11). H_{int} and M_Q data are normalized at $P=0$ [H_{int}=2.5 kOe and $M_Q \sim 0.8\mu_B$ (∗) or $0.6\mu_B$ (☆)]. The energy gap $2\Delta_0/k_BT_c$ as a function of P is estimated from a decreasing rate in $1/T_1$ below T_c(●) and the specific-heat jump at T_c(○) using the relation $\Delta C = -D(E_F)\frac{d\Delta^2(T)}{dT}|_{T=T_c}$ (Ref. 4). Here, the values of $2\Delta_0/k_BT_c$ obtained from the specific-heat measurements are normalized as they fit the values obtained from the NQR measurements between 2.1 and 2.5 GPa. The solid lines are guides to the eyes.

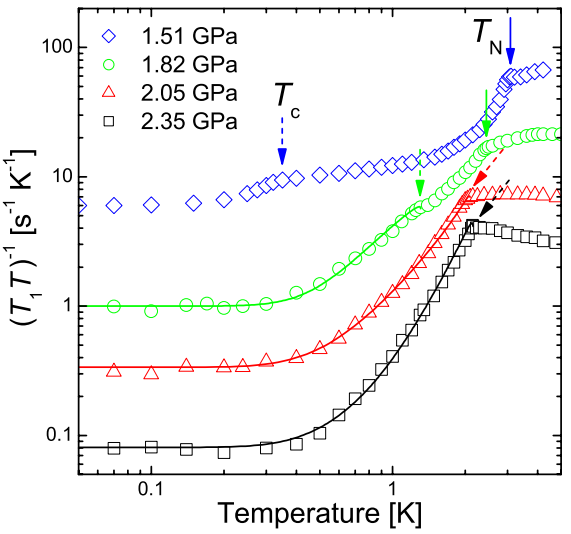

FIG. 4. (Color online) The T dependences of $(T_1T)^{-1}$ at pressures above 1.51 GPa. For clarity, note that the $(T_1T)^{-1}$ data at 1.82, 2.05, and 2.35 GPa are divided by 3, 9, and 18, respectively. The solid and the dashed arrows indicate T_N and T_c, respectively. The solid curves represent fitting curves with parameters $2\Delta_0/k_BT_c$ and RDOS (see text).

2.5 kOe at $P=0$ to 1.6 kG at $P=1.67$ GPa and M_Q decreases from $0.6\mu_B$ at $P=0$ to $0.43\mu_B$ at $P=1.7$ GPa, revealing the relation for $H_{int}^{In(2)} \propto M_Q$ in $P=0-1.67$ GPa where the incommensurate domains are dominant. When $P=1.76-2.05$ GPa, where the commensurate AFM is completely established over the entire sample, it is demonstrated that M_Q markedly decreases from $0.36\mu_B$ at $P=1.76$ GPa to $0.2\mu_B$ at $P=2.02$ GPa by using the relation of $H_{int}^{In(2)} \propto M_Q$. This result leads us to deduce that, at the microscopic level, the SC coexists with the commensurate AFM near the QCP. Figure 3(c) shows the P dependence of the SC energy gap $2\Delta_0/k_BT_c$, which was deduced from the T dependence of $(T_1T)^{-1}$ below T_c using the $d_{x^2-y^2}$-wave model [$\Delta(\theta,\phi)=\Delta_0 \cos 2\phi$] with parameters $2\Delta_0/k_BT_c$ and the residual density of states (RDOS) at the Fermi level. Here, the RDOS is normalized by the density of states at the Fermi level in the PM state. From the best fitting curves indicated by the solid lines in Fig. 4, we obtained sets of parameters $(2\Delta_0/k_BT_c, \text{RDOS}) = (4.2, 0.42)$, (5.45,0.22), and (6.6,0.14) at 1.82, 2.05, and 2.35 GPa, respectively. As shown in Fig. 3(c), the strong coupling SC is realized above the AFM-QCP in $CeRhIn_5$, which is similar to that in $CeCoIn_5$.[19] In $CeCoIn_5$, where the AFM order is absent and the coexistence of AFM and SC is not observed, the RDOS which is mainly derived from the impurity effect is almost constant for P.[19] However, the RDOS rapidly increases with decreasing P below the AFM-QCP in $CeRhIn_5$, as shown in Fig. 4, suggesting the gapless nature inherent to the coexistence of AFM and SC.[7,8] An important finding presented here is that $2\Delta_0/k_BT_c$ and T_c increase with a significant decrease in M_Q above 1.76 GPa, which provides evidence of strong coupling between the commensurate AFM and the SC OPs.

It is to be noted that the commensurate AFM domains exist even at $P=0$ since the central peak is observed in the NQR spectrum at the bottom of Fig. 2(a). This fraction VF_c is as small as 3–4 % of the sample used here. However, VF_c has been confirmed to decrease with an improvement in the quality of the sample. This result suggests that the contamination of the commensurate AFM domains at $P=0$ is possibly associated with the existence of inner stress that is inevitably introduced in the sample, for instance, near the surface region of $CeRhIn_5$. Therefore, it is assumed that the change in the magnetic structure of $CeRhIn_5$ is also sensitive to the existence of strains in the sample introduced by a large pres-

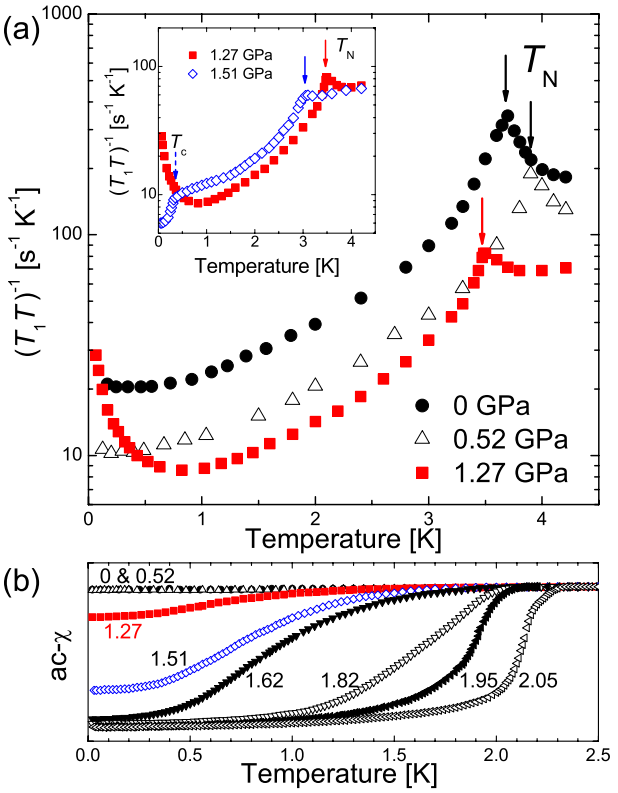

FIG. 5. (Color online) (a) The T dependences of $(T_1T)^{-1}$ on the In(1) site for $P=0$, 0.52, and 1.27 GPa. The inset shows the T dependences of $(T_1T)^{-1}$ for $P=1.27$ and 1.51 GPa. (b) The T dependences of the ac susceptibility between $P=0$ GPa and 2.05 GPa obtained by using the *in situ* NQR coil. The ac susceptibility is normalized by its value at 2.4 K for each pressure. The fact that the ac susceptibility at $T=0$ is saturated above P_m suggests that the full SC diamagnetism is realized above P_m.

sure gradient in the pressure cell. In one study, Fluorinert-70/77 that freezes at the room temperature near $P=1$ GPa was used in neutron experiments performed at P.[20] The observation of a rise in Q_z from 0.297 to 0.4 at $P=1$ GPa may be due to the very large pressure gradient brought about by the application of pressure in the frozen pressure-transmitting medium. It may be difficult to observe commensurate AFM during the neutron-scattering measurements since the Ce magnetic moments rapidly decrease above P_m.

It has been demonstrated from the present NQR measurements that SC uniformly coexists with the commensurate AFM and that both OPs are strongly coupled. Another issue is whether the SC can exist in incommensurate AFM. Figure 5(a) shows the T dependence of $(T_1T)^{-1}$ below P_m in order to discuss the SC behavior for incommensurate AFM. $(T_1T)^{-1}$ below 0.52 GPa shows a critical slowing down of spin fluctuations at T_N and a $(T_1T)^{-1}$-constant behavior well below T_N, representing the characteristics for metallic antiferromagnets. In this P region, the ac susceptibility does not exhibit SC diamagnetism at all, as shown in Fig. 5(b). However, a marked enhancement of $(T_1T)^{-1}$ below 0.6 K and the SC diamagnetism of approximately 16% were observed at 1.27 GPa, where the incommensurate AFM is still dominant. These results suggest that the superconducting correlation starts to develop around 1.27 GPa, but its effect seems to be confined to a short range since the decrease in $(T_1T)^{-1}$ due to the occurrence of the bulk SC was not found down to the lowest T, as shown in Fig. 5(a). The enhancement of $(T_1T)^{-1}$ at 1.27 GPa may be induced by SC fluctuations in the incommensurate AFM.

The NQR results mentioned above indicate that there can be two possible scenarios for the SC phenomenon in the incommensurate AFM. One is when the bulk SC appears in the incommensurate AFM. In this case, the SC-QCP exists around 1.27 GPa and T_c continuously starts to increase from 0 K above the SC-QCP. However, it is difficult to verify the occurrence of the bulk SC in the incommensurate AFM below P_m since the specific-heat jump greatly decreases below 1.7 GPa.[4,21] If it is true that bulk SC appears even in the incommensurate AFM, theoretical studies are necessary to explain why the specific-heat jump at T_c is very small in the coexisting phase of the incommensurate AFM and SC. Another scenario is when the bulk SC does not appear, but instead the SC correlation is confined to a short range in the incommensurate AFM below P_m. It is possible that the incommensurate AFM prevents the development of SC OP. The incommensurate helical magnetic structure, as seen in Fig. 1(a), may suppress the growth in the SC correlation along the c axis in $CeRhIn_5$. As a result, bulk SC does not occur in the incommensurate AFM below P_m. Whichever scenario is true, it is remarkable that the SC correlation starts to develop even in the incommensurate AFM regime around 1.27 GPa.

IV. CONCLUSION

In conclusion, systematic measurements of the ^{115}In-NQR spectrum have revealed that commensurate AFM with $Q_c=(\frac{1}{2},\frac{1}{2},\frac{1}{2})$ takes place uniformly over the entire sample above $P_m\sim1.7$ GPa near QCP at $P=2.1$ GPa. It is reinforced in the microscopic level that the SC uniformly coexists with the commensurate AFM in such a manner that the magnitude of SC OP and T_c increase as the AFM-ordered moment is reduced. This result provides evidence of strong coupling between the commensurate AFM OP and the SC OP. The observation of short-range SC correlation even in the incommensurate AFM regime at 1.27 GPa requires further theoretical studies on the SC characteristics in the incommensurate AFM. The present experiments have shed light on interplay between magnetism and SC in strongly correlated electron systems.

ACKNOWLEDGMENTS

This work was supported by a Grant-in-Aid for Specially Promoted Research (Grant No. 20001004) and it was also partially supported by the Global COE Program (Core Research and Engineering of Advanced Materials-Interdisciplinary Education Center for Materials Science) from the Ministry of Education, Culture, Sports, Science and Technology (MEXT), Japan. M.Y. was supported by a Grant-in-Aid for Young Scientists (B) of MEXT (Grant No. 20740175).

*Present address: Department of Physics, Kyoto University, Kyoto 606-8502, Japan.

[1] W. Bao, P. G. Pagliuso, J. L. Sarrao, J. D. Thompson, Z. Fisk, J. W. Lynn, and R. W. Erwin, Phys. Rev. B **62**, R14621 (2000).

[2] H. Hegger, C. Petrovic, E. G. Moshopoulou, M. F. Hundley, J. L. Sarrao, Z. Fisk, and J. D. Thompson, Phys. Rev. Lett. **84**, 4986 (2000).

[3] T. Muramatsu, N. Tateiwa, T. C. Kobayashi, K. Shimizu, K. Amaya, D. Aoki, H. Shishido, Y. Haga, and Y. Ōnuki, J. Phys. Soc. Jpn. **70**, 3362 (2001).

[4] G. Knebel, D. Aoki, D. Braithwaite, B. Salce, and J. Flouquet, Phys. Rev. B **74**, 020501(R) (2006).

[5] T. Park, F. Ronning, H. Q. Yuan, M. B. Salamon, R. Movshovich, J. L. Sarrao, and J. D. Thompson, Nature (London) **440**, 65 (2006).

[6] T. Mito, S. Kawasaki, Y. Kawasaki, G.-q. Zheng, Y. Kitaoka, D. Aoki, Y. Haga, and Y. Ōnuki, Phys. Rev. Lett. **90**, 077004 (2003).

[7] S. Kawasaki, T. Mito, Y. Kawasaki, G.-q. Zheng, Y. Kitaoka, D. Aoki, Y. Haga, and Y. Ōnuki, Phys. Rev. Lett. **91**, 137001 (2003).

[8] M. Yashima, S. Kawasaki, H. Mukuda, Y. Kitaoka, H. Shishido, R. Settai, and Y. Ōnuki, Phys. Rev. B **76**, 020509(R) (2007).

[9] A. Llobet, J. S. Gardner, E. G. Moshopoulou, J.-M. Mignot, M. Nicklas, W. Bao, N. O. Moreno, P. G. Pagliuso, I. N. Goncharenko, J. L. Sarrao, and J. D. Thompson, Phys. Rev. B **69**, 024403 (2004).

[10] S. Majumdar, G. Balakrishnan, M. R. Lees, D. McK. Paul, and G. J. McIntyre, Phys. Rev. B **66**, 212502 (2002).

[11] S. Raymond, G. Knebel, D. Aoki, and J. Flouquet, Phys. Rev. B **77**, 172502 (2008).

[12] A. Llobet, A. D. Christianson, W. Bao, J. S. Gardner, I. P. Swainson, J. W. Lynn, J.-M. Mignot, K. Prokes, P. G. Pagliuso, N. O. Moreno, J. L. Sarrao, J. D. Thompson, and A. H. Lacerda, Phys. Rev. Lett. **95**, 217002 (2005).

[13] M. Yokoyama, H. Amitsuka, K. Matsuda, A. Gawase, N. Oyama, I. Kawasaki, K. Tenya, and H. Yoshizawa, J. Phys. Soc. Jpn. **75**, 103703 (2006).

[14] S. Ohira-Kawamura, H. Shishido, A. Yoshida, R. Okazaki, H. Kawano-Furukawa, T. Shibauchi, H. Harima, and Y. Matsuda, Phys. Rev. B **76**, 132507 (2007).

[15] T. Mito, S. Kawasaki, G.-q. Zheng, Y. Kawasaki, K. Ishida, Y. Kitaoka, D. Aoki, Y. Haga, and Y. Ōnuki, Phys. Rev. B **63**, 220507(R) (2001).

[16] A. S. Kirichenko, A. V. Kornilov, and V. M. Pudalov, Instrum. Exp. Tech. **48**, 813 (2005).

[17] N. J. Curro, P. C. Hammel, P. G. Pagliuso, J. L. Sarrao, J. D. Thompson, and Z. Fisk, Phys. Rev. B **62**, R6100 (2000).

[18] G. F. Chen, K. Matsubayashi, S. Ban, K. Deguchi, and N. K. Sato, Phys. Rev. Lett. **97**, 017005 (2006).

[19] M. Yashima, S. Kawasaki, Y. Kawasaki, G.-q. Zheng, Y. Kitaoka, H. Shishido, R. Settai, Y. Haga, and Y. Ōnuki, J. Phys. Soc. Jpn. **73**, 2073 (2004).

[20] V. A. Sidorov and R. A. Sadykov, J. Phys.: Condens. Matter **17**, S3005 (2005).

[21] G. Knebel, M.-A. Méasson, B. Salce, D. Aoki, D. Braithwaite, J. P. Brison, and J. Flouquet, J. Phys.: Condens. Matter **16**, 8905 (2004).